molecular pharmaceutics

pubs.acs.org/molecularpharmaceutics Article

Ferritin-Displayed GLP-1 with Improved Pharmacological Activities and Pharmacokinetics

Wencheng Su,[⊥] Huanbo Tan,[⊥] Robert Janowski, Wenyu Zhang, Pengju Wang, Jie Zhang, Huanhuan Zhai, Jian Li, Dierk Niessing, Michael Sattler, and Peijian Zou*

Cite This: *Mol. Pharmaceutics* 2020, 17, 1663−1673 Read Online

ACCESS | Metrics & More | Article Recommendations | Supporting Information

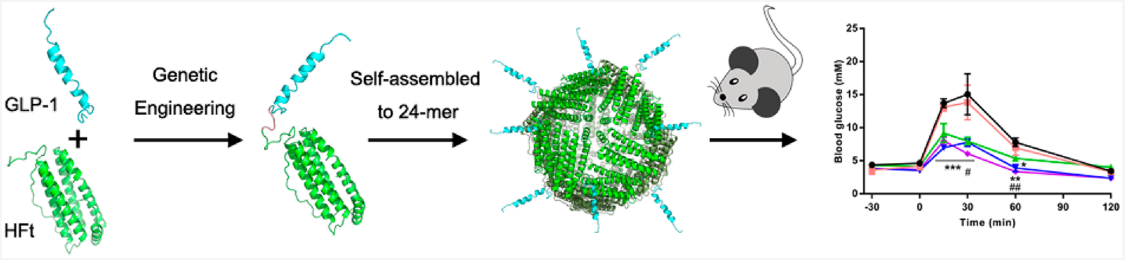

ABSTRACT: Glucagon-like peptide-1 (GLP-1) is an incretin (a type of metabolic hormone that stimulates a decrease in blood glucose levels), holding great potential for the treatment of type 2 diabetes mellitus (T2DM). However, its extremely short half-life of 1−2 min hampers any direct clinical application. Here, we describe the application of the heavy chain of human ferritin (HFt) nanocage as a carrier to improve the pharmacological properties of GLP-1. The GLP-HFt was designed by genetic fusion of GLP-1 to the N-terminus of HFt and was expressed in inclusion bodies in *E. coli*. The refolding process was developed to obtain a soluble GLP-HFt protein. The biophysical properties determined by size-exclusion chromatography (SEC), dynamic light scattering (DLS), circular dichroism (CD), transmission electron microscopy (TEM), and X-ray crystallography verified that the GLP-HFt successfully formed a 24-mer nanocage with GLP-1 displayed on the external surface of HFt. The *in vivo* pharmacodynamic results demonstrated that the GLP-HFt nanocage retained the bioactivity of natural GLP-1, significantly reduced the blood glucose levels for at least 24 h in a dose-dependent manner, and inhibited food intake for at least 8−10 h. The half-life of the GLP-HFt nanocage was approximately 52 h in mice after subcutaneous injection. The prolonged half-life and sustained control of blood glucose levels indicate that the GLP-HFt nanocage can be further developed for the treatment of T2DM. Meanwhile, the HFt nanocage proves its great potential as a universal carrier that improves the pharmacodynamic and pharmacokinetic properties of a wide range of therapeutic peptides and proteins.

KEYWORDS: *diabetes, glucagon-like peptide-1, ferritin, bioactivities, half-life*

INTRODUCTION

Diabetes is one of the largest threats to global health in the 21st century. Data from the International Diabetes Federation (IDF) shows that a total of 425 million people (aged 20−79 years) worldwide suffer from diabetes, and the number is expected to increase to 629 million by 2045.[1] Cases of type 2 diabetes mellitus (T2DM), characterized by insulin resistance and, consequently, impaired β cell function and hyperglycemia, account for 90−95% of people affected with diabetes.[2,3] It is reported that obesity promotes insulin resistance by alteration of metabolic and endocrine functions in adipose tissue,[4] and 80−90% of T2DM patients are obese.[5] Therefore, a challenge in drug development for T2DM treatment is that effective therapy should also show potential for weight reduction.

Glucagon-like peptide-1 (GLP-1) is an incretin, secreted from the intestinal L cells after food digestion.[6] GLP-1 exerts its functions through binding to the GLP-1 receptor, belonging to the class B family of G protein-coupled receptors (GPCR), mainly expressed in pancreatic β-cells and also in the central nervous system, lungs, stomach, heart, and kidneys.[7,8] GLP-1 is involved in many pharmacological activities beneficial for glucose control, such as stimulation of insulin secretion in a glucose-dependent manner, inhibition of glucagon secretion, induction of β-cell proliferation, delaying of gastric emptying rate, and inhibition of food intake.[8−10] Given this versatility, GLP-1 is considered to be an ideal agent for the treatment of T2DM and obesity.

Received: January 30, 2020
Revised: April 2, 2020
Accepted: April 3, 2020
Published: April 3, 2020

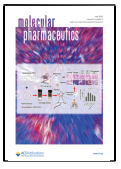

https://dx.doi.org/10.1021/acs.molpharmaceut.0c00098
Mol. Pharmaceutics 2020, 17, 1663−1673

However, the application of GLP-1 in the clinic is limited by the short half-life ($T_{1/2}$), less than 2 min, of active forms of GLP-1, GLP-1(7−36) amide, and GLP-1(7−37). This is caused by rapid degradation by dipeptidyl peptidase-4 (DPP-4) and kidney clearance.[11,12] Inspired by its great application potential, ongoing efforts have been made to improve the stability of GLP-1 in the bloodstream, resulting in several GLP-1R agonists being approved by the FDA or EMA. To improve the pharmacokinetic profiles of GLP-1, chemical modification of sequence and genetic fusion to albumin or IgG-Fc are the two most applied strategies. The liraglutide and semaglutide are produced by the addition of a fatty acid chain for HSA binding.[13] The albiglutide and dulaglutide are designed by genetic fusion of modified GLP-1 to albumin or IgG-Fc, resulting in a long half-life through the neonatal Fc receptor (FcRn)-dependent recycling system.[3,14] One general strategy for stability improvement is to replace the second amino acid Ala8 with one that cannot be recognized by DPP-4, such as Gly (albiglutide and dulaglutide) or unnatural Aib (semaglutide). Alternatively, exendin-4, isolated from the venom of the Gila monster and sharing 53% sequence homology with the native GLP-1, has been also modified (exenatide, lixisenatide, and extended-release exenatide).[10] Although approved drugs are available, more efforts are being put into developing new drugs for the treatment of T2DM and obesity, due to a large number of patients and the unmet clinical needs.

Ferritin (Ft) is an iron storage protein with a nanocage structure.[15] Each Ft nanocage comprises 24 subunits, which self-assemble to form a cage-like nanostructure with an outer diameter of roughly 12 nm and an inner diameter of 8 nm.[16] Ft exhibits remarkable thermal and chemical stability, good biodegradability, biocompatibility, high solubility, and low toxicity properties.[17,18] In addition, the uniform cage size of Ft allows for the loading of relatively even amounts of a delivery drug.[18] Furthermore, Ft can be expressed in *E. coli* with high yield in a soluble form.[19] For this reason, Ft nanocages have been extensively applied by loading drugs and chemical agents into the internal cavities or by displaying peptides, proteins, or antibody fragments on the exterior surface through genetic fusion or chemical conjugation.[16,20,21] Human Ft is a heteropolymer consisting of heavy (H) and light (L) chains. Previous studies have demonstrated that recombinant Ft heavy-chain (HFt) nanocages show a well-assembled structure and retain consistent iron-storage activity and drug delivery capacity.[22,23]

To improve the pharmacodynamic properties of GLP-1, we developed a novel GLP-1R agonist by the genetic fusion of GLP-1 to the N-terminus of an HFt monomer through a short linker. Subsequent self-assembly of the HFt nanocage structure presents 24 GLP-1 peptides on the surface. We denoted this as GLP-HFt. We report here the uniformity, bioactivity, and half-life of the resultant GLP-HFt nanocage evaluated *in vivo* and *in vitro*.

EXPERIMENTAL SECTION

Design of GLP-HFt. The HFt gene, based on the amino acid sequence (UniProt no. P02794), was synthesized by GenScript (Nanjing, China), taking into consideration codon optimization for high-level expression in *E. coli*, and further ligated into a modified pET-24d(+) plasmid with *Nco*I/*Eco*RI restriction sites to construct expression vector (pET-24d-HFt) by polymerase chain reaction (PCR) amplification. The gene sequence, encoding the modified GLP-1 (7−37) with A8G mutation to prevent degradation by DPP-4, was also synthesized by GenScript. We constructed the pET-24d-GLP-HFt expression vector by fusing the GLP-1 sequence to the N-terminus of HFt through a flexible linker composed of Gly-Ser-Gly-Gly-Gly. The pET-24d-GLP-HFt plasmid contained an N-terminal TEV (tobacco etch virus) protease cleavage site for the removal of the additional methionine (Met).

Expression and Purification of Recombinant HFt and GLP-HFt. The pET-24d-HFt and pET-24d-GLP-HFt plasmids were transformed into *E. coli* BL21(DE3) for expression of the intended proteins. Transformed cells were grown at 37 °C to an OD_{600} of 0.6 in LB medium containing 50 μg/mL of kanamycin (Solarbio, Beijing, China). The cultures were then induced by 1 mM of IPTG (Sigma-Aldrich, Shanghai, China) at 25 °C for 4 h. After induction, cells were harvested by centrifugation at 5000 rpm for 25 min, and the pellets were suspended in buffer A (25 mM Tris-HCl, pH 7.4), homogenized by a high-pressure homogenizer (ATS, Taizhou, China) for three cycles with a pressure of 800−900 bar, and then centrifuged at 14 000 rpm for 60 min at 4 °C.

The HFt supernatant was collected to be purified through a previously established method[17] with some modifications. In brief, the disrupted supernatant was heated to 60 °C for 10 min, and the precipitate was removed by centrifugation. The residual supernatant was purified by anion-exchange chromatography on a Q-Sepharose Fast Flow column (HiTrap Q HP, GE Healthcare, USA), pre-equilibrated with 25 mM Tris-HCl, pH 7.4, followed by elution with 25 mM Tris-HCl, 0.32 M NaCl, pH 7.4. The eluted protein was further purified by gel filtration (HiPrep 16/60 Sephacryl S-400 HR, GE Healthcare, USA). The purified HFt protein was analyzed by SDS-PAGE and Native-PAGE and stored at −80 °C for further use.

The inclusion bodies (IBs) from GLP-HFt cell lysates were washed twice with buffer B (25 mM Tris-HCl, 1 mM EDTA, 1% Triton X-100, pH 7.4) and once with buffer C (25 mM Tris-HCl, 1 mM EDTA, pH 7.4). The IBs were solubilized by incubation in buffer C, containing 2 M urea, at 25 °C for 3 h, and then refolded at 25 °C by dialyzing against 0 M urea in buffer C overnight. The soluble GLP-HFt protein was cleaved with TEV protease to remove the Met at the N-terminus of GLP-1 and then heated to 60 °C for 10 min. The precipitate was removed by centrifugation. Finally, the supernatant protein was concentrated using an Amicon Ultra device (Millipore, USA) over a 30 kDa cutoff filter and then isolated by gel filtration (HiPrep 16/60 Sephacryl S-400 HR, GE Healthcare, USA). The yield and purity of recombinant HFt and GLP-HFt proteins were analyzed by 12% SDS-PAGE and 6% Native-PAGE. The concentration of HFt and GLP-HFt proteins was determined in triplicate by the BCA protein assay kit (CWBIO, Beijing, China) using bovine serum albumin (BSA) as the standard.

Biophysical Characterization of HFt and GLP-HFt Proteins. The prepared HFt and GLP-HFt proteins were characterized by size-exclusion chromatography (SEC), dynamic light scattering (DLS), circular dichroism (CD), transmission electron microscopy (TEM), and X-ray crystallography.

Size-Exclusion Chromatography. SEC analysis was performed on an ÄKTA purifier system (GE Healthcare, USA). One mL of protein solution was loaded on the gel filtration column (HiPrep 16/60 Sephacryl S-400 HR), which was pre-equilibrated with 25 mM Tris-HCl at pH 7.4 and eluted at 0.5

https://dx.doi.org/10.1021/acs.molpharmaceut.0c00098
Mol. Pharmaceutics 2020, 17, 1663−1673

mL/min. The elution profile of GLP-HFt was monitored by measuring absorbance at 280 nm.

Dynamic Light Scattering. The HFt and GLP-HFt protein samples (100 μL, 1 mg/mL) were prepared in phosphate buffer (20 mM, pH 7.4), centrifugated at 12 000 rpm for 10 min, and were then equilibrated at 25 °C. A Brookhaven 90Plus Particle Size Analyzer (Brookhaven Instruments Corporation, USA) was used to perform DLS analysis.

CD Spectrum. A total of 200 μL of HFt and GLP-HFt (0.5 mg/mL) were dissolved in phosphate buffer (20 mM, pH 7.4) and injected into a 1.0 mm path length quartz cuvette. The CD spectra of HFt and GLP-HFt were obtained on a Chirascan-plus CD spectrometer (Applied Photophysics, U.K.) at 25 °C. The spectra were measured from 180 to 260 nm. Every sample was scanned three times, and the data were averaged.

Transmission Electron Microscopy. For TEM observations, the HFt and GLP-HFt protein samples were exchanged to phosphate buffer (10 mM, pH 7.0). Ten μL of HFt or GLP-HFt protein was embedded in the Plasma Cleaner HPDC32G treated carbon−copper grid and absorbed for 10 min; then the excess solution was removed with filter paper. The copper grids of covered samples were washed with ddH_2O and stained with 1% phosphotungstic acid for 5 min and then imaged at 80 kV through an HT7700 scanning electron microscope (Hitachi, Japan).

Crystallization and X-ray Structural Analysis. To confirm the assembly of GLP-HFt into a 24-mer nanocage, we performed crystallization and X-ray diffraction analysis. The crystallization experiments for GLP-HFt were performed at the X-ray Crystallography Platform at Helmholtz Zentrum München. The crystallization screening was done at 292 K using 16 mg/mL of protein with a Mosquito (SPT Labtech) nanodrop dispenser in sitting-drop 96-well plates and commercial screens. The crystals of GLP-HFt grew in 0.1 M HEPES buffer, pH 7.5, and 20% (v/v) Jeffamine M-600. For the X-ray diffraction experiments, crystals were mounted in a nylon fiber loop and flash-cooled to 100 K in liquid nitrogen. Prior to freezing, cryoprotection was performed for three seconds in a reservoir solution complemented with 30% (v/v) ethylene glycol. X-ray diffraction tests were performed on the SLS PXIII X06DA beamline (PSI, Villigen), and all measurements were performed at 100 K.

Animals. The male C57BL/6 mice (20−25 g) and female BALB/c mice (20−25 g) were all obtained from the Academy of Military Medical Science (Beijing, China). The animals were housed under a 12:12 h light−dark cycle, and the temperature of the environment was maintained at 24 ± 2 °C with free access to food and water throughout the acclimatization, except where noted. All experiments were carried out following the guideline principles for the care and use of laboratory animals approved by the Animal Care Committee of China.

Oral Glucose Tolerance Test (OGTT). In order to verify whether the GLP-HFt nanocage improved the glucose tolerance of mice, OGTTs were performed as described by Finan et al.,[24] with some modifications. Briefly, after one-week acclimatization, the male C57BL/6 mice were fasted overnight (14−16 h) and then weighed. The mice were randomly divided into five groups based on their body weight (n = 5 per group): placebo (Tris buffer), HFt (33 nmol/kg), and GLP-HFt (10, 33, and 100 nmol/kg) groups. The proteins were then injected subcutaneously 30 min before the oral glucose challenge (2 g of glucose per kg body weight). Mice in the control group received the same volume of placebo. Blood glucose levels were measured by a OneTouch UltraEasy glucometer (Johnson & Johnson, USA) at −30, 0, 15, 30, 60, and 120 min after the glucose load.

The OGTT was also conducted 24 h after subcutaneous injection. The mice were randomly divided into five groups: placebo, GLP-HFt (10, 33, and 100 nmol/kg), and liraglutide (33 nmol/kg) group. The food was measured from 0 to 8 h, and then food intake was calculated by the food decrease (g)/body weight (bw, g). Other procedures were performed as described above.

Feeding Studies and Nonfasting Blood Glucose Measurements. The male C57BL/6 mice were grouped according to their body weight (n = 5 per group) followed by fasting overnight (14−16 h). A single dose of 33 mol/kg GLP-HFt nanocage was administered subcutaneously. Mice in the control group were given the same volume of placebo. The mice were then placed into individual cages containing the preweighed rodent chow with free access to water. The food was measured at the time preset, and then food intake was calculated by the food decrease (g)/body weight (bw, g). The nonfasting blood glucose was measured by a OneTouch UltraEasy glucometer at different time points after administration.

Effects on Streptozotocin (STZ)-Induced Diabetic Mice. The diabetic C57BL/6 mice (20 g) were induced by intraperitoneal injection of STZ (45 mg/kg/day in citrate buffer, pH 4.5, with an injection volume of 0.2 mL) for 5 consecutive days after being fasted overnight. After another 7 days, 44 out of 50 mice with nonfasting blood glucose exceeding 11.1 mM were considered to be diabetic. After overnight fasting, the mice were randomly assigned to 4 treatment groups (n = 5 per group). Subcutaneous injection of the placebo and the different doses of GLP-HFt (10, 33, and 100 nmol/kg) solution followed. The plasma glucose levels were measured by a OneTouch UltraEasy glucometer at different time points after administration.

Labeling of HFt and GLP-HFt Nanocages. FITC-labeled HFt and GLP-HFt were prepared according to the protocol provided by Sigma-Aldrich (Shanghai, China). In brief, the FITC was dissolved in anhydrous DMSO at 1 mg/mL; then, 50 μL of FITC solution was added to 2 mg/mL HFt and GLP-HFt solution in 1 mL of carbonate/bicarbonate (pH 9.0). The mixture was incubated at 4 °C overnight. A final concentration of 50 mM of NH_4Cl was added to stop the reaction. The unbound FITC was separated using a Hitrap Desalting column (GE Healthcare, USA) pre-equilibrated with 10 mM PB. FITC-conjugated HFt and GLP-HFt were concentrated by centrifugation at 4000 rpm for 20 min, using a Vivaspin-4 Centrifugal Concentrator (MWCO 100 kDa, Sartorius). UV−vis spectroscopy (Nanodrop 2000, ThermoFisher) was performed to determine the concentration of FITC in conjugated nanocages. Protein concentrations of FITC-labeled HFt and GLP-HFt were measured using a BCA protein assay kit (CWBIO, Beijing, China).

Pharmacokinetic Analysis. The female BALB/c mice were used to determine pharmacokinetic properties as described by Fan et al.,[25] with some modifications. The FITC-labeled HFt and GLP-HFt (100 μg/mouse) were subcutaneously injected into the BALB/c mice (n = 3 for each group). At different time points (30 min, 1, 2, 4, 8, 10, 24, 48, 72, and 96 h) after injection, 20 μL of blood was collected from the tail vein and dropped into an Ep tube containing EDTA-Na_2 anticoagulant. The blood sample mixture was

https://dx.doi.org/10.1021/acs.molpharmaceut.0c00098
Mol. Pharmaceutics 2020, 17, 1663−1673

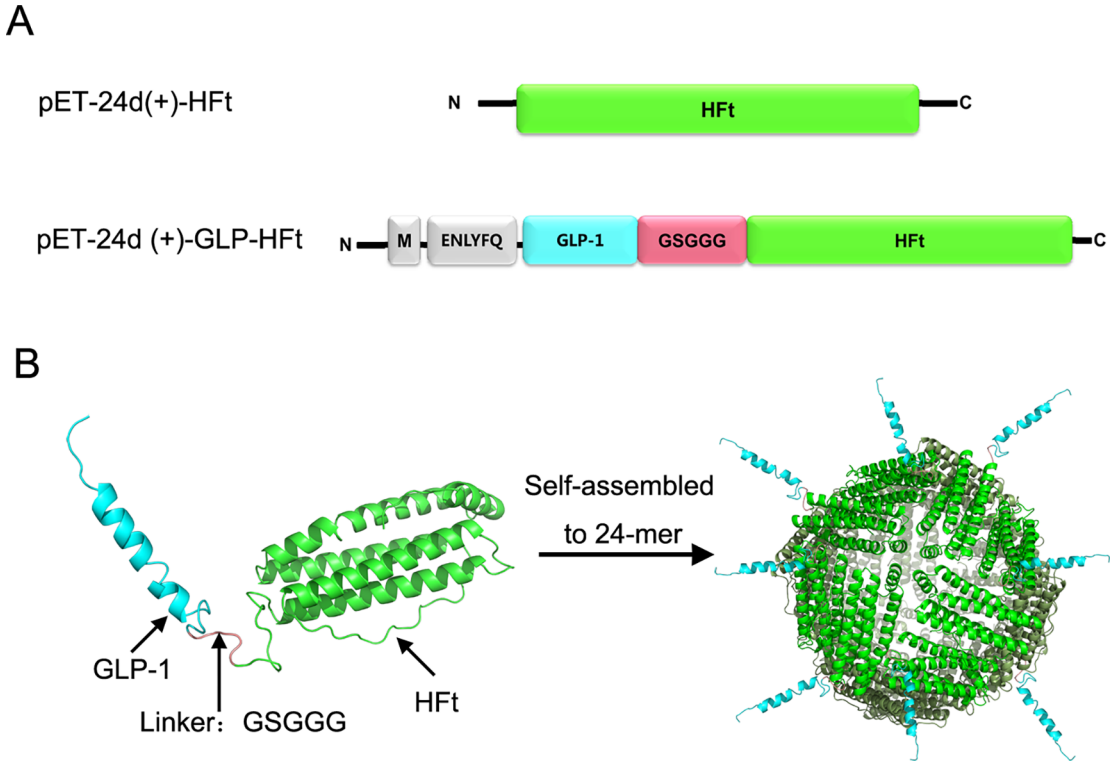

Figure 1. Schematic description of GLP-HFt. (A) GLP-1 was genetically fused to the N-terminus of the HFt through a flexible linker. A TEV cleavage site was inserted between methionine (M) and GLP-1. (B) Schematic representation of the self-assembly and supermolecular assembly processes of GLP-HFt fusion protein constructs.

centrifuged at 4000 rpm for 15 min to separate the plasma. The plasma samples were stored at −80 °C and kept away from light until subsequent procedures. To detect the FITC-labeled nanocages, 10 μL of plasma was diluted with 90 μL of Tris/HCl buffer (25 mM, pH 7.0) in a black 96-well plate (Costar, Corning, USA), followed by analysis with a SpectraMax M2 microplate reader (Molecular Devices, USA) using excitation at 485 nm and emission at 535 nm. To correct for nonspecific background fluorescence, the fluorescence of blood samples from untreated mice was also determined. The plasma concentrations of FITC-labeled HFt and GLP-HFt were calculated according to the standard curves. Non-compartmental analysis of the final data was performed using the PK Solver Excel Add-in program[26] to calculate half-life.[27]

Statistical Analysis. The analyses were performed using GraphPad Prism 5.0 for Windows (GraphPad Software, CA, USA), and the data were presented as mean ± SEM. Statistical analyses were performed using the one-way or two-way analysis of variance (ANOVA) followed by Tukey's multiple comparison analysis. A p-value of less than 0.05 was considered to be statistically significant.

RESULTS

Construction and Generation of HFt and GLP-HFt. To improve the pharmacokinetic and pharmacodynamic properties of GLP-1, the GLP-1 peptide was genetically fused to the N-terminus of HFt (~21 kDa as a monomer), referred to as GLP-HFt (Figure 1A). A TEV protease recognition site was inserted between the Met and the GLP-1 to produce a free N-terminus of GLP-1 after the proteinase cleavage, which was indispensable for bioactivity. The native HFt is a 24-mer nanocage. A modeling simulation of the GLP-HFt monomer was generated using the ModWeb system.[28] The GLP-1, fused to the N-terminus of HFt, displayed on the surface of the nanocage, as shown in the model (Figure 1B).

The recombinant HFt and GLP-HFt nanocages were successfully expressed and purified in accordance with previous reports,[17,22] with some modifications. The HFt was expressed in the soluble fraction and purified by heating, anion-exchange, and size-exclusion chromatography. The recombinant GLP-HFt proteins were abundantly expressed in the insoluble fraction. Alterations of the IPTG induction conditions did not improve the solubility of the GLP-HFt fusion protein (data not shown). It was found that the inclusion bodies could be resolubilized in 2 M urea, possibly because the protein was only partially misfolded. The urea was removed by a dialysis procedure to obtain the soluble and folded protein. The Met at the N-terminus of the GLP-HFt protein was then removed by TEV protease to obtain the free N-terminus of GLP-1 (Figure 2A). The GLP-HFt was further purified by heating and size-exclusion chromatography. As shown in Figure 2B, the purified HFt and GLP-HFt subunits appeared on the reduced SDS-PAGE as single bands of approximately 21 kDa and 25 kDa, respectively, consistent with the theoretical size of the recombinant proteins. The Native-PAGE exhibited only a single band (Figure 2C), indicating that purified HFt and GLP-HFt were of high purity and homogeneity. The ultimate yields were 80 mg per 1000 mL cell culture for HFt and 35 mg for GLP-HFt.

Structural Characterization of HFt and GLP-HFt. To fully characterize the recombinant HFt and GLP-HFt nanocage, SEC, DLS, CD, TEM, and X-ray diffraction analysis were performed. SEC analysis by a Sephacryl S-400 HR column demonstrated that both the HFt and GLP-HFt showed one

https://dx.doi.org/10.1021/acs.molpharmaceut.0c00098
Mol. Pharmaceutics 2020, 17, 1663−1673

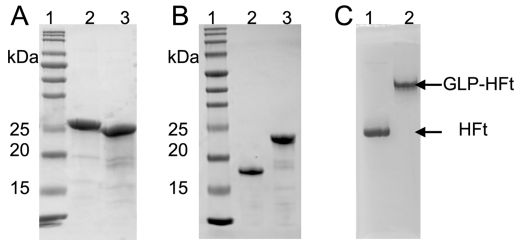

Figure 2. SDS-PAGE and Native PAGE analyses of HFt and GLP-HFt. (A) The cleaved GLP-HFt with TEV protease was analyzed by 12% SDS-PAGE. Lane 1, marker; lane 2, GLP-HFt; lane 3, the cleaved GLP-HFt. (B) The purified HFt and GLP-HFt were analyzed by 12% SDS-PAGE. 1, marker; lane 2, HFt; lane 3, GLP-HFt. (C) The purified HFt and GLP-HFt were analyzed by 6% Native-PAGE. Lane 1, HFt; lane 2, GLP-HFt.

main peak, suggesting a highly monodisperse character. The recombinant GLP-HFt was eluted earlier than the HFt, exhibiting a relatively larger hydrodynamic radius (Figure 3A). This indicates that the GLP-HFt formed a stable 24-mer nanocage architecture, similar to HFt. In addition, in order to further confirm the monodispersity of HFt and GLP-HFt and to clarify whether the GLP-1 was successfully displayed on the surface of the nanocage, DLS analyses were conducted. It was shown that the mean diameters of HFt and GLP-HFt were 13.7 and 14.7 nm, respectively (Figure 3C,D). The exhibited diameter of GLP-HFt was larger than that of HFt, and this result can be ascribed to the introduced GLP-1 located on the particle surface.

Crystal structures show that both HFt protein and GLP-1 are mainly α-helical in their secondary structure.[29,30] We detected possible differences in the secondary structure between HFt and GLP-HFt proteins by far-UV CD spectroscopy. The CD spectrum of HFt exhibited the typical features of an α-helical protein with two characteristic minima around 209 and 222 nm (Figure 3B), which was in good agreement with literature reports that ferritin is rich in α-helices.[31] The CD spectrum revealed that the GLP-HFt nanocage retained the α-helical structure, but exhibited a slight deviation, possibly resulting from the addition of GLP-1, which also has an α-helical structure. This indicates that GLP-1 at the N-terminus of HFt hardly affects the folding of HFt.

To further confirm whether GLP-1 interfered with the assembly of the HFt nanocage, the morphology of HFt and GLP-HFt was observed by the TEM method. The TEM images showed that GLP-HFt has a globular shape resembling the cage-like architecture of HFt (Figure 4). The diameter of

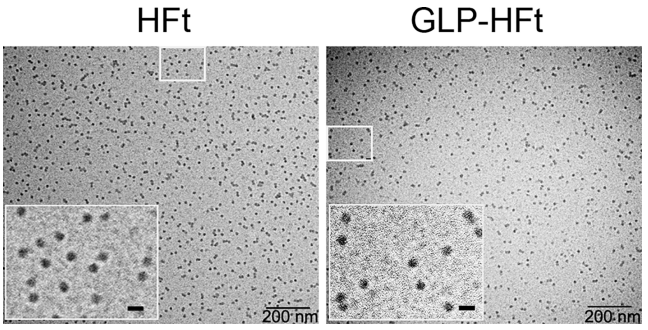

Figure 4. Transmission electron microscopy (TEM) images of 1% phosphotungstic acid-stained HFt and GLP-HFt nanocages. The inserts show the magnification, in which scale bars represent 20 nm.

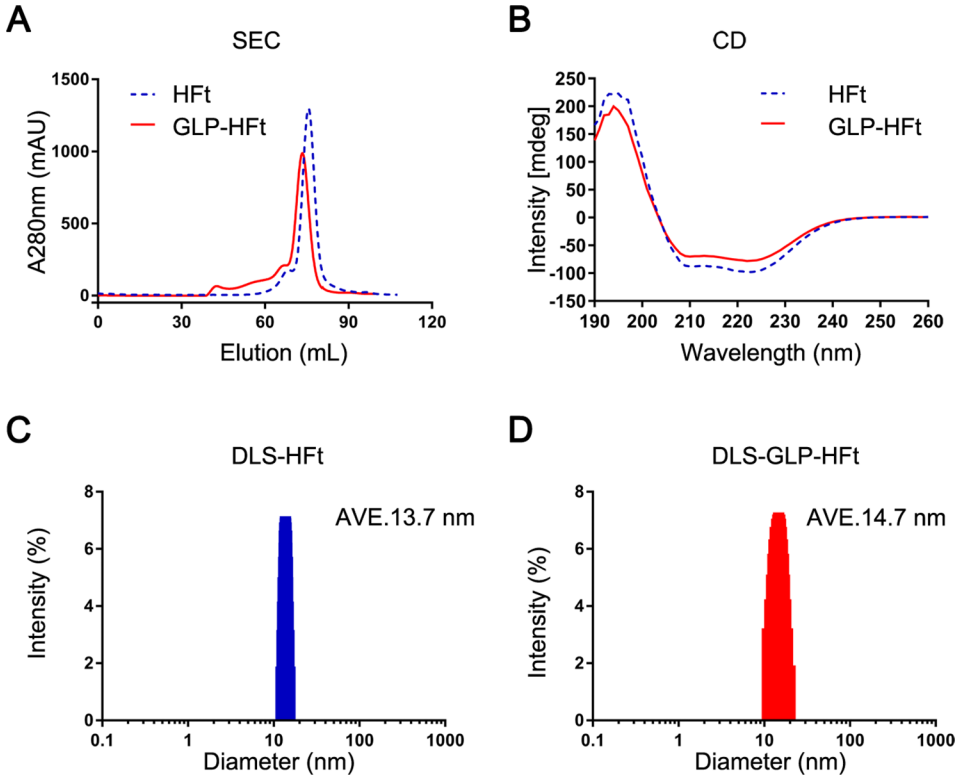

Figure 3. Structural characterizations of the purified HFt and GLP-HFt nanocages. (A) Size-exclusion chromatography. (B) Circular dichroism. (C, D) Dynamic light scattering.

https://dx.doi.org/10.1021/acs.molpharmaceut.0c00098
Mol. Pharmaceutics 2020, 17, 1663−1673

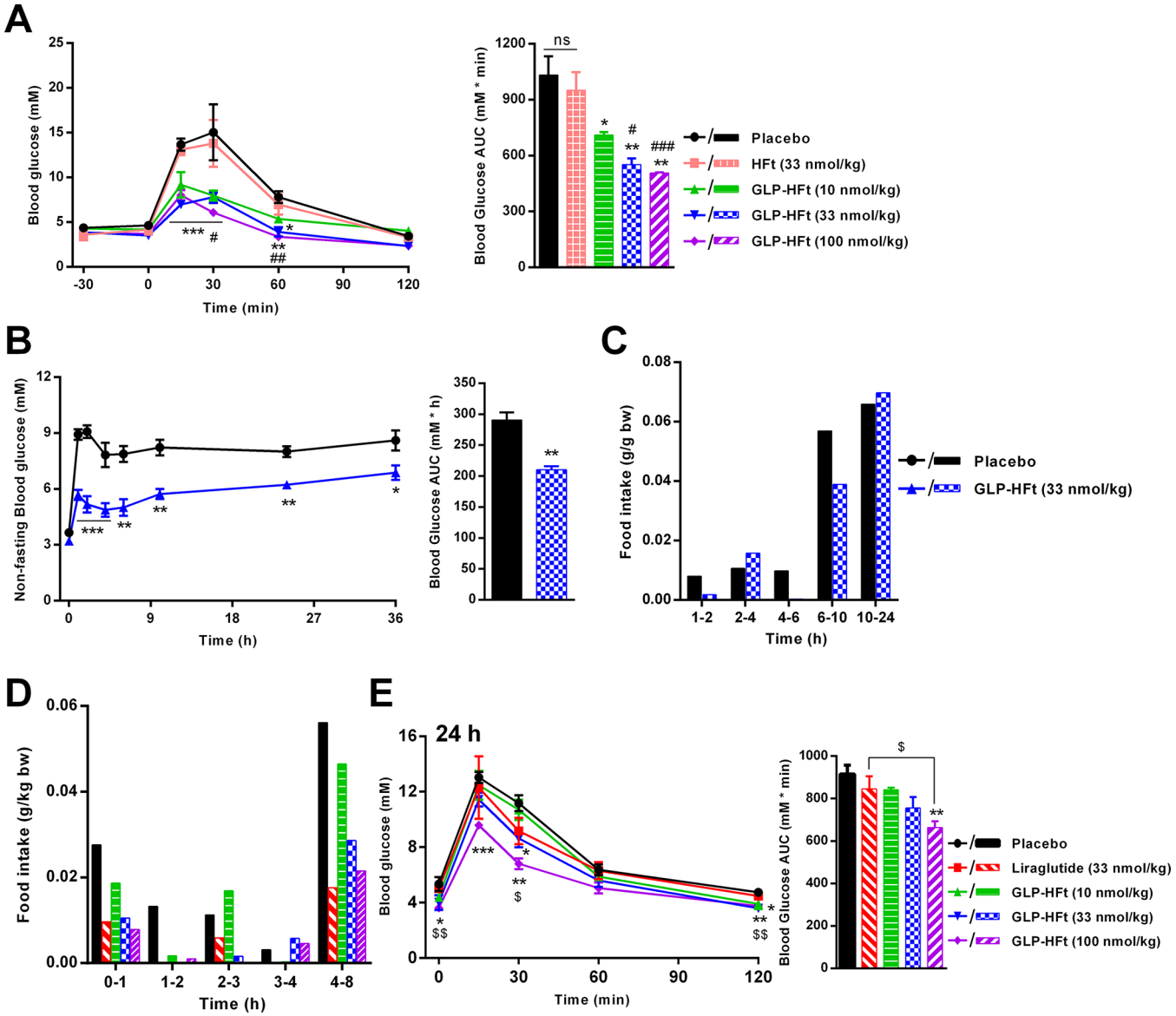

Figure 5. Effects of the GLP-HFt nanocage on blood glucose and food intake. (A) Blood glucose levels and area under the curve (AUC) during OGTT in mice. The mice were fasted overnight (14−16 h) and then subcutaneously injected with GLP-HFt nanocage at a dose of 10, 33, and 100 nmol/kg, and then, blood glucose levels were measured. (B and C) Blood glucose levels, AUC (B), and food intake (C) after one single injection of the GLP-HFt nanocage at a dose of 33 nmol/kg. (D) Food intake of mice treated with different concentrations of GLP-HFt and liraglutide. (E) Blood glucose levels and AUC during OGTT performed 24 h after subcutaneous injection of the GLP-HFt nanocage (10, 33, and 100 nmol/kg) and liraglutide (33 nmol/kg). Data are presented as mean ± SEM, n = 5 mice. * $p < 0.05$, ** $p < 0.01$, *** $p < 0.001$ for test groups versus the placebo group. $^{\#}$ $p < 0.05$, $^{\#\#}$ $p < 0.01$, $^{\#\#\#}$ $p < 0.001$ for the GLP-HFt (100 nmol/kg) group versus the 10 nmol/kg group. $^{\$}$ $p < 0.05$, $^{\$\$}$ $p < 0.01$ for the GLP-HFt (100 nmol/kg) group versus the liraglutide group. The "ns" represented no significance.

GLP-HFt, calculated from the TEM image, was larger (∼13.6 nm) than that of HFt (∼11.9 nm), in accordance with the DSL results. These results indicate that GLP-1 is correctly presented on the surface of HFt and does not affect the formation of an intact nanocage architecture for GLP-HFt.

Finally, the GLP-HFt was crystallized, and X-ray diffraction data was obtained from the crystals using the SLS PXIII X06DA beamline (PSI, Villigen). Although the tested crystals exhibited rather poor quality and we did not manage to collect a full data set, from the preliminary X-ray diffraction analysis, we were able to calculate the unit cell parameters of a = 146.8 Å, b = 218.8 Å, and c = 218.8 Å. By comparing the unit cell parameters to other ferritin structures and additionally by searching the Protein Data Bank for crystal structures with similar unit cell parameters, we can state that GLP-HFt assembles into a 24-mer nanocage. When using the range of the unit cell parameters a = 215−220 Å, b = 215−220 Å, and c = 140−150 Å, we found only 3 PDB entries: human H-chain ferritin mutant-MBP,[32] human H-chain ferritin with an extension peptide (PDB 6J4A), and the structures of mouse H-chain-modified ferritin (PDB 3WNW). All three structures exhibit 24-mer assembly.

Effects of GLP-HFt on Blood Glucose *in Vivo*. To confirm that GLP-HFt retained the bioactivity of native GLP-1 *in vivo*, blood glucose levels were measured after injection. In the oral glucose tolerance test (OGTT), different concentrations of GLP-HFt (10, 33, and 100 nmol/kg) were injected subcutaneously into mice 30 min before the glucose challenge

https://dx.doi.org/10.1021/acs.molpharmaceut.0c00098
Mol. Pharmaceutics 2020, 17, 1663−1673

(2 g/kg). The results showed that GLP-HFt significantly improved glucose tolerance, reducing blood glucose levels in a dose-dependent manner. GLP-HFt, at a dose of 100 nmol/kg, was the most potent in the blood-glucose-lowering effect. There was no significant difference observed between HFt and the placebo (Figure 5A), suggesting that HFt had no effect on blood glucose. This indicates that the blood-glucose-lowering effect of GLP-HFt was derived solely from the GLP-1 on the surface of the nanocage.

To clarify how long GLP-HFt could control the blood glucose level *in vivo*, continuous detection was conducted. GLP-HFt was subcutaneously injected once into fasted mice at a dose of 33 nmol/kg; then the nonfasting blood glucose levels from 0 to 36 h were measured. The results demonstrated that the duration of action of GLP-HFt was considerably prolonged, lowering blood glucose levels for 36 h (Figure 5B). That was remarkably longer than the effect of GLP-1(8G), also with an A8G mutation, which showed blood glucose reduction for only 0.5 h at a dose of 50 nmol/kg in mice.[33] To further confirm the prolonged action, we compared GLP-HFt and liraglutide, an FDA-approved drug for the treatment of T2DM developed by Novo Nordisk with a once-daily injection. The OGTTs were performed 24 h after administration of liraglutide and different concentrations of GLP-HFt. After 24 h, liraglutide (33 nmol/kg) and GLP-HFt (10 nmol/kg) had no significant blood-glucose-lowering effect. The GLP-HFt at a dose of 33 nmol/kg significantly reduced the blood glucose at 30 and 120 min. The calculated AUC for HLP-HFt (33 nmol/kg) was lower than liraglutide with an equivalent dose, though without statistical significance. GLP-HFt at a dose of 100 nmol/kg had the most striking effect on blood glucose. At 0, 30, and 120 min, GLP-HFt (100 nmol/kg) was more potent, resulting in a much lower AUC value, compared with liraglutide (Figure 5E). These results indicate that GLP-HFt still dose-dependently improved glucose tolerance 24 h after administration.

Effects of GLP-HFt on Food Intake. To verify that the GLP-HFt nanocage retains the bioactivity of food intake inhibition, food intake after subcutaneous administration was measured. After a single injection at a dose of 33 nmol/kg, the GLP-HFt nanocage decreased food intake for at least 10 h compared with the placebo (0.04 g/kg bw versus 0.06 g/kg bw, Figure 5C). HFt alone had no significant food intake inhibitory effect (Figure S1). In the dose−response study, GLP-HFt dose-dependently reduced food intake from 0 to 8 h. Liraglutide (33 nmol/kg) also inhibited food intake for 8 h. At 8 h, the consumption of food per milligram body weight was 0.06, 0.02, 0.05, 0.03, and 0.02 for the placebo, liraglutide, and GLP-HFt nanocage (10, 33, and 100 nmol/kg), respectively (Figure 5D).

Effects of GLP-HFt on STZ-Induced Diabetic Mice. To further confirm the application prospect of the GLP-HFt nanocage for T2DM treatment, diabetic mice were induced by STZ. The nonfasting blood glucose levels in the diabetic mice were all above 11.1 mM. The effects of GLP-HFt on STZ-induced diabetic mice are shown in Figure 6. The GLP-HFt nanocage dose-dependently reduced the nonfasting blood glucose of the STZ-induced diabetic mice. At both doses of 10 and 33 nmol/kg, the GLP-HFt nanocage significantly reduced blood glucose for 6 h. At 10 h, GLP-HFt at a dose of 100 nmol/kg still significantly reduced blood glucose (Figure 6A). The calculated AUC for GLP-HFt (100 nmol/kg) was much lower than that of 10 nmol/kg from 0 to 10 h (Figure 6B). HFt alone had no significant blood-glucose-lowering effect (Figure S2).

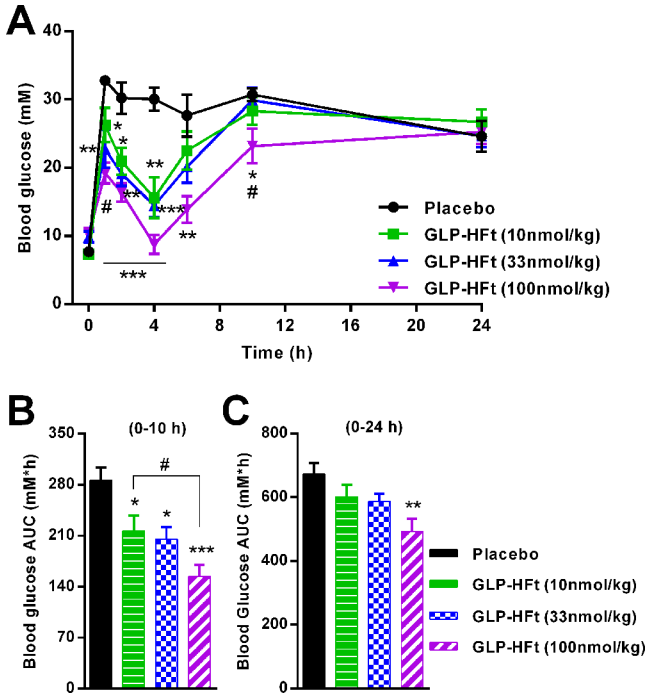

Figure 6. Effects of the GLP-HFt nanocage on blood glucose in STZ-induced diabetic mice. The diabetic mice were fasted overnight (14−16 h) followed by subcutaneous injection of the GLP-HFt nanocage at a dose of 10, 33, and 100 nmol/kg. Then, the blood glucose levels (A) were measured, and the AUC_{0-10h} (B) and AUC_{0-24h} (C) were calculated. Data are presented as mean ± SEM, $n = 5$ mice. * $p < 0.05$, ** $p < 0.01$, *** $p < 0.001$ for GLP-HFt groups versus the placebo group. # $p < 0.05$ for GLP-HFt (100 nmol/kg) group versus 10 nmol/kg group.

Pharmacokinetics of GLP-HFt *in Vivo*. To determine the half-lives of HFt and GLP-HFt nanocages, FITC was used to label the recombinant proteins. The mice were given single doses of FITC-labeled HFt and GLP-HFt via subcutaneous administration, and then the plasma was examined for fluorescence. The calculated half-lives of FITC-labeled HFt and GLP-HFt were 51.1 and 51.9 h, respectively, without statistical significance (Figure 7). The long half-lives may be the result of slow absorbance by the capillaries after subcutaneous injection due to the large hydrodynamic diameter, 13−14 nm.

■ DISCUSSION

The Ft nanocage has been found to exist almost ubiquitously in nature and is highly conserved from prokaryotes to eukaryotic animals. The naturally derived Ft nanocage is stable in physiological conditions and is biocompatible. Ft typically shows low immunogenicity in biomedical applications.[34,35] Consequently, the Ft nanocage has been extensively modified and developed as a drug-carrier delivery system[18] to display many peptides and proteins by genetic fusion or chemical conjugation, such as the albumin-binding domain (ABD),[17] PAS,[23] RGD4C,[21] XTEN-affibody,[19] Nanobody,[25] epidermal growth factor (EGF),[22] citrine,[36] tumor-specific antigen,[37] influenza viral hemeagglutinin (HA),[38] and antibody.[39,40] The coverage of molecules bound to Ft is wide, from small peptides to large proteins, and from simple to complex. The Ft-modified

https://dx.doi.org/10.1021/acs.molpharmaceut.0c00098
Mol. Pharmaceutics 2020, 17, 1663−1673

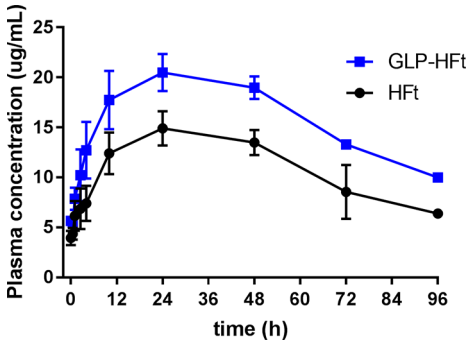

Figure 7. Plasma concentrations of HFt and GLP-HFt nanocages in BALB/c mice. The FITC was used to label the HFt and GLP-HFt nanocages. The mice were then given 100 μg of FITC-labeled HFt and GLP-HFt nanocages via subcutaneous administration; then the fluorescence in plasma was detected.

therapeutics showed a longer circulation half-life or improved pharmacological activity.

Herein, we designed a novel GLP-HFt nanocage by genetic fusion of GLP-1 to the N-terminus of the heavy chain of human ferritin (HFt) that might be suitable for human treatment *in vivo*. We expected that the HFt nanocage, with its large diameter, could improve the pharmacodynamic and pharmacokinetic properties of GLP-1 by reducing renal filtration and increasing potency based on the 24-mer structure.

The previous studies showed that HFt nanocage with an N-terminal fused ABD or a PAS polypeptide was expressed in *E. coli* as a soluble protein; however, EGF-fused HFt was only found in inclusion bodies.[17,22,23] This may be related to the biochemical characteristics of the fusion partner. Here, the GLP-HFt was found to be insoluble in *E. coli* and could not form a spherical shell. We found that 2 M urea could resolubilize the aggregates. The denatured proteins were refolded into the active form by removing the urea via dialysis. The 2 M urea was of a much lower concentration than the 8 M urea used in the refolding of EGF-FTH1 and was much easier to remove.[22] In comparison with the other therapy-approved GLP-1R agonists, which are usually produced by chemical synthesis or via yeast or mammalian cells with high cost and long-period, the GLP-HFt nanocage expressed in *E. coli* using the genetic fusion strategy is relatively simple and of low cost.[41] This denaturation-refolding process is versatile and could be applied to other protein cages.[22]

We observed that GLP-HFt formed a nanocage and successfully displayed GLP-1 on the surface. The biophysical characterization of GLP-HFt determined by CD and TEM demonstrated that the 24-mer architecture was successfully formed, comparable to HFt. The DSL and SEC results showed that GLP-HFt was slightly larger compared with native HFt, suggesting that the GLP-1 was exhibited on the surface of the nanocage, facilitating binding to GLP-1R. We could not procure the complete crystal structure data of the GLP-HFn nanocage, perhaps because of the flexible linker and the large motions of GLP-1, which result in frequent deformation by crystal contacts. A comparison of the unit cell parameters to the other ferritin structures, however, indicated that GLP-HFt assembles into a 24-mer nanocage. These results indicate that fusion of GLP-1 to the N terminus of the HFt subunit does not interfere with the self-assembly of the subunits to form the characteristic 24-subunit protein cage architecture of HFt. Our results were in agreement with previous studies, which demonstrated that Ft is very stable due to large numbers of salt bridges and hydrogen bonds,[42] and the ability for self-assembly is retained, even when fused to an influenza virus hemeagglutinin with a molecular weight above 60 kDa.[38]

The GLP-1R agonists approved by the FDA or EMA usually contain one or two GLP-1 molecules.[10,43] The GLP-HFt nanocage exhibited 24 GLP-1 molecules on the external surface. We anticipated that more GLP-1 molecules in one assembly would translate to higher bioactivity and a longer half-life *in vivo*. The results showed that the GLP-HFt nanocage had a dose-dependent efficacy and duration of action of up to 36 h, quite long compared with the duration of GLP-1 (8G), which was only 0.5 h.[33] We further evaluated the efficacy of the GLP-HFt nanocage compared with FDA-approved liraglutide by OGTT. After 24 h, the GLP-HFt nanocage still exerted a significant blood-glucose-lowering effect, while the liraglutide showed no significant effect. We also evaluated GLP-HFt antidiabetic activity in STZ-induced diabetic mice, and results demonstrated that nonfasting blood glucose was significantly reduced in GLP-HFt-treated mice. These results suggest that the GLP-HFt nanocage retains the natural bioactivity of binding and activation of GLP-1R and also indicate that the HFt nanocage remarkably prolonged the bioactivity of GLP-1 *in vivo*. It is noteworthy that all 24 of the GLP-1 molecules may not have had the opportunity to bind to a GLP-1 receptor, due to steric hindrance resulting from the large molecular size of the nanocage. The GLP-HFt nanocage may not exert maximum bioactivity, as there may be some competition and interference in the binding process. This interference could probably be reduced by a more rational structural design and a proper decrease in the number of GLP-1 molecules.

One advantage of GLP-1 is its inhibitory effect on food intake, resulting in weight loss, which is beneficial for T2DM treatment. Liraglutide, in two 56-week clinical trials, at a dose of 3 mg, led to a reduction of 6.4−8.4 kg of body weight in overweight or obese patients, while the placebo led to a reduction of only 2.2−2.8 kg.[44,45] Therefore, liraglutide was approved for the treatment of T2DM at a dose of 1.2 mg or 1.8 mg per day followed by approval for weight management at a dose of 3.0 mg per day.[46] In the current study, the GLP-HFt nanocage reduced food intake for at least 8−10 h. This inhibitory effect was long-acting, indicating that the GLP-HFt nanocage retains the native biological activity of GLP-1, and might assist weight loss in patients with diabetes.

This sustainable efficacy of GLP-HFt might be attributable to the long half-life of approximately 52 h in mice. The HFt nanocage allowed for half-life extension of GLP-1, perhaps mainly because of the large hydrodynamic diameter (13.7 nm for HFt and 14.7 nm for GLP-HFt nanocage), resulting in slowed renal clearance. Previous studies have demonstrated that the threshold of renal filtration for globular proteins is approximately 5−6 nm in hydrodynamic diameter. A particle larger than 6 nm will be excreted more slowly, resulting in prolonged retention time in circulation.[47,48] Another reason for the long half-life might be attributable to slow absorption by capillaries at the injection site after subcutaneous administration. The effective pore size in a normal, intact vascular endothelium is approximately 5 nm. A particle with a hydrodynamic diameter greater than 5 nm transports slowly across the endothelium, leading to a longer time needed to achieve an equilibrium between the vascular compartment and

https://dx.doi.org/10.1021/acs.molpharmaceut.0c00098
Mol. Pharmaceutics 2020, 17, 1663−1673

the extravascular extracellular space.[48] The slow absorption resulted in a maximum plasma concentration (C_{max}) 24 h after injection and a long flat plasma concentration profile before reaching a linear elimination phase. The slowed absorption was favorable for maintaining the plasma concentration of GLP-HFt in an efficacious range.

Furthermore, the prolonged half-life of GLP-HFt may be ascribed to the GLP-1 exhibited on the surface, acting as a shield, decreasing, to some extent, HFt receptor-mediated cell uptake and endocytosis because of increased steric hindrance. Previous studies have shown that rapid degradation by enzymes and receptor-mediated cell uptake and endocytosis cause the short half-life of native HFt, which is only 2 h in mice after intravenous injection.[17] Surface coverage of PEG, PAS, or XTEN sequences has been proven to be effective for half-life extension of HFt due to surface shielding.[19,23,49]

Taken together, the reduced renal clearance, slowed absorption, and increased steric hindrance give GLP-HFt improved pharmacokinetic properties. However, it is noteworthy that the slowed absorption rate might lead to a relatively low plasma concentration. Therefore, a relatively high dose may be required for the initial injection to cause a sufficient reduction in blood glucose.

CONCLUSION

In summary, a novel GLP-1R agonist based on the HFt nanocage was designed. The generated GLP-HFt successfully formed a nanocage architecture resembling the native HFt nanocage. The GLP-HFt nanocage retained the bioactivities of native GLP-1, significantly reducing blood glucose levels and inhibiting food intake. The pharmacokinetic profile of GLP-HFt was remarkably improved due to slowed absorption and reduced renal clearance when compared to GLP-1 alone. Our data indicate that the GLP-HFt nanocage may hold great promise for the treatment of T2DM and obesity. In addition, the HFt nanocage shows promising potential as a universal carrier for half-life extension and drug delivery.

ASSOCIATED CONTENT

Supporting Information

The Supporting Information is available free of charge at https://pubs.acs.org/doi/10.1021/acs.molpharmaceut.0c00098.

GLP-HFt nanocage inhibited food intake; effects of HFt on blood glucose in STZ-induced diabetic mice (PDF)

AUTHOR INFORMATION

Corresponding Author

Peijian Zou − *Industrial Enzymes National Engineering Laboratory, Tianjin Institute of Industrial Biotechnology, Chinese Academy of Sciences, 300308 Tianjin, China; Institute of Structural Biology, Helmholtz Zentrum Muenchen, German Research Center for Environmental Health, 85764 Neuherberg, Germany; Center for Integrated Protein Science Munich at Chair Biomolecular NMR Spectroscopy, Department Chemie, Technische Universität München, 85747 Garching, Germany;* orcid.org/0000-0002-7561-8310; Email: peijian.zou@tum.de, zou_pj@tib.cas.cn

Authors

Wencheng Su − *Industrial Enzymes National Engineering Laboratory, Tianjin Institute of Industrial Biotechnology, Chinese Academy of Sciences, 300308 Tianjin, China*

Huanbo Tan − *Industrial Enzymes National Engineering Laboratory, Tianjin Institute of Industrial Biotechnology, Chinese Academy of Sciences, 300308 Tianjin, China*

Robert Janowski − *Institute of Structural Biology, Helmholtz Zentrum Muenchen, German Research Center for Environmental Health, 85764 Neuherberg, Germany*

Wenyu Zhang − *Industrial Enzymes National Engineering Laboratory, Tianjin Institute of Industrial Biotechnology, Chinese Academy of Sciences, 300308 Tianjin, China*

Pengju Wang − *Industrial Enzymes National Engineering Laboratory, Tianjin Institute of Industrial Biotechnology, Chinese Academy of Sciences, 300308 Tianjin, China*

Jie Zhang − *Industrial Enzymes National Engineering Laboratory, Tianjin Institute of Industrial Biotechnology, Chinese Academy of Sciences, 300308 Tianjin, China*

Huanhuan Zhai − *Industrial Enzymes National Engineering Laboratory, Tianjin Institute of Industrial Biotechnology, Chinese Academy of Sciences, 300308 Tianjin, China*

Jian Li − *Industrial Enzymes National Engineering Laboratory, Tianjin Institute of Industrial Biotechnology, Chinese Academy of Sciences, 300308 Tianjin, China*

Dierk Niessing − *Institute of Structural Biology, Helmholtz Zentrum Muenchen, German Research Center for Environmental Health, 85764 Neuherberg, Germany; Institute of Pharmaceutical Biotechnology, Ulm University, 89081 Ulm, Germany*

Michael Sattler − *Industrial Enzymes National Engineering Laboratory, Tianjin Institute of Industrial Biotechnology, Chinese Academy of Sciences, 300308 Tianjin, China; Institute of Structural Biology, Helmholtz Zentrum Muenchen, German Research Center for Environmental Health, 85764 Neuherberg, Germany; Center for Integrated Protein Science Munich at Chair Biomolecular NMR Spectroscopy, Department Chemie, Technische Universität München, 85747 Garching, Germany;* orcid.org/0000-0002-1594-0527

Complete contact information is available at: https://pubs.acs.org/10.1021/acs.molpharmaceut.0c00098

Author Contributions

⊥W.S. and H.T. contributed equally to this work.

Notes

The authors declare no competing financial interest.

ACKNOWLEDGMENTS

This work was supported by the National Natural Science Foundation of China (31800649) and the Youth Innovation Promotion Association, the Chinese Academy of Sciences (2018211). Mr. Gregory Patrick Wolfe is much appreciated for proofreading this paper.

REFERENCES

(1) International Diabetes Federation. *IDF Diabetes Atlas*, 8th ed.; 2017; pp 1−147

(2) American Diabetes, A.. Diagnosis and classification of diabetes mellitus. *Diabetes Care* **2014**, *37* (Suppl 1), S81−S90.

(3) Alavi, S. E.; Cabot, P. J.; Moyle, P. M. Glucagon-Like Peptide-1 Receptor Agonists and Strategies To Improve Their Efficiency. *Mol. Pharmaceutics* **2019**, *16*, 2278−2295.

(4) Zhou, J. Y.; Poudel, A.; Welchko, R.; Mekala, N.; Chandramani-Shivalingappa, P.; Rosca, M. G.; Li, L. Liraglutide improves insulin sensitivity in high fat diet induced diabetic mice through multiple pathways. *Eur. J. Pharmacol.* **2019**, *861*, 172594.
(5) Evers, A.; Bossart, M.; Pfeiffer-Marek, S.; Elvert, R.; Schreuder, H.; Kurz, M.; Stengelin, S.; Lorenz, M.; Herling, A.; Konkar, A.; Lukasczyk, U.; Pfenninger, A.; Lorenz, K.; Haack, T.; Kadereit, D.; Wagner, M. Dual Glucagon-like Peptide 1 (GLP-1)/Glucagon Receptor Agonists Specifically Optimized for Multidose Formulations. *J. Med. Chem.* **2018**, *61*, 5580−5593.
(6) Baggio, L. L.; Drucker, D. J. Biology of incretins: GLP-1 and GIP. *Gastroenterology* **2007**, *132*, 2131−2157.
(7) Moon, M. J.; Park, S.; Kim, D. K.; Cho, E. B.; Hwang, J. I.; Vaudry, H.; Seong, J. Y. Structural and molecular conservation of glucagon-like Peptide-1 and its receptor confers selective ligand-receptor interaction. *Front. Endocrinol. (Lausanne, Switz.)* **2012**, *3*, 141.
(8) Cho, Y. M.; Merchant, C. E.; Kieffer, T. J. Targeting the glucagon receptor family for diabetes and obesity therapy. *Pharmacol. Ther.* **2012**, *135*, 247−248.
(9) Lorenz, M.; Evers, A.; Wagner, M. Recent progress and future options in the development of GLP-1 receptor agonists for the treatment of diabesity. *Bioorg. Med. Chem. Lett.* **2013**, *23*, 4011−4018.
(10) Brown, E.; Cuthbertson, D. J.; Wilding, J. P. Newer GLP-1 receptor agonists and obesity-diabetes. *Peptides* **2018**, *100*, 61−67.
(11) Drucker, D. J. Biological actions and therapeutic potential of the glucagon-like peptides. *Gastroenterology* **2002**, *122*, 531−544.
(12) Deacon, C. F.; Hughes, T. E.; Holst, J. J. Dipeptidyl peptidase IV inhibition potentiates the insulinotropic effect of glucagon-like peptide 1 in the anesthetized pig. *Diabetes* **1998**, *47*, 764−769.
(13) Knudsen, L. B.; Lau, J. The Discovery and Development of Liraglutide and Semaglutide. *Front. Endocrinol. (Lausanne, Switz.)* **2019**, *10*, 155.
(14) Roopenian, D. C.; Akilesh, S. FcRn: the neonatal Fc receptor comes of age. *Nat. Rev. Immunol.* **2007**, *7*, 715−725.
(15) Jutz, G.; van Rijn, P.; Santos Miranda, B.; Boker, A. Ferritin: a versatile building block for bionanotechnology. *Chem. Rev.* **2015**, *115*, 1653−1701.
(16) He, D.; Marles-Wright, J. Ferritin family proteins and their use in bionanotechnology. *New Biotechnol.* **2015**, *32*, 651−657.
(17) Wang, C.; Zhang, C.; Li, Z.; Yin, S.; Wang, Q.; Guo, F.; Zhang, Y.; Yu, R.; Liu, Y.; Su, Z. Extending Half Life of H-Ferritin Nanoparticle by Fusing Albumin Binding Domain for Doxorubicin Encapsulation. *Biomacromolecules* **2018**, *19*, 773−781.
(18) Maham, A.; Tang, Z.; Wu, H.; Wang, J.; Lin, Y. Protein-based nanomedicine platforms for drug delivery. *Small* **2009**, *5*, 1706−1721.
(19) Lee, N. K.; Lee, E. J.; Kim, S.; Nam, G. H.; Kih, M.; Hong, Y.; Jeong, C.; Yang, Y.; Byun, Y.; Kim, I. S. Ferritin nanocage with intrinsically disordered proteins and affibody: A platform for tumor targeting with extended pharmacokinetics. *J. Controlled Release* **2017**, *267*, 172−180.
(20) Zang, J.; Chen, H.; Zhao, G.; Wang, F.; Ren, F. Ferritin cage for encapsulation and delivery of bioactive nutrients: From structure, property to applications. *Crit. Rev. Food Sci. Nutr.* **2017**, *57*, 3673−3683.
(21) Zhen, Z.; Tang, W.; Chen, H.; Lin, X.; Todd, T.; Wang, G.; Cowger, T.; Chen, X.; Xie, J. RGD-modified apoferritin nanoparticles for efficient drug delivery to tumors. *ACS Nano* **2013**, *7*, 4830−4837.
(22) Li, X.; Qiu, L.; Zhu, P.; Tao, X.; Imanaka, T.; Zhao, J.; Huang, Y.; Tu, Y.; Cao, X. Epidermal growth factor-ferritin H-chain protein nanoparticles for tumor active targeting. *Small* **2012**, *8*, 2505−2514.
(23) Falvo, E.; Tremante, E.; Arcovito, A.; Papi, M.; Elad, N.; Boffi, A.; Morea, V.; Conti, G.; Toffoli, G.; Fracasso, G.; Giacomini, P.; Ceci, P. Improved Doxorubicin Encapsulation and Pharmacokinetics of Ferritin-Fusion Protein Nanocarriers Bearing Proline, Serine, and Alanine Elements. *Biomacromolecules* **2016**, *17*, 514−522.
(24) Finan, B.; Yang, B.; Ottaway, N.; Smiley, D. L.; Ma, T.; Clemmensen, C.; Chabenne, J.; Zhang, L.; Habegger, K. M.; Fischer, K.; Campbell, J. E.; Sandoval, D.; Seeley, R. J.; Bleicher, K.; Uhles, S.; Riboulet, W.; Funk, J.; Hertel, C.; Belli, S.; Sebokova, E.; Conde-Knape, K.; Konkar, A.; Drucker, D. J.; Gelfanov, V.; Pfluger, P. T.; Muller, T. D.; Perez-Tilve, D.; DiMarchi, R. D.; Tschop, M. H. A rationally designed monomeric peptide triagonist corrects obesity and diabetes in rodents. *Nat. Med.* **2015**, *21*, 27−36.
(25) Fan, K.; Jiang, B.; Guan, Z.; He, J.; Yang, D.; Xie, N.; Nie, G.; Xie, C.; Yan, X. Fenobody: A Ferritin-Displayed Nanobody with High Apparent Affinity and Half-Life Extension. *Anal. Chem.* **2018**, *90*, 5671−5677.
(26) Zhang, Y.; Huo, M. R.; Zhou, J. P.; Xie, S. F. PKSolver: An add-in program for pharmacokinetic and pharmacodynamic data analysis in Microsoft Excel. *Comput. Methods Programs Biomed.* **2010**, *99*, 306−314.
(27) Jacobs, S. A.; Gibbs, A. C.; Conk, M.; Yi, F.; Maguire, D.; Kane, C.; O'Neil, K. T. Fusion to a highly stable consensus albumin binding domain allows for tunable pharmacokinetics. *Protein Eng., Des. Sel.* **2015**, *28*, 385−393.
(28) Eswar, N.; John, B.; Mirkovic, N.; Fiser, A.; Ilyin, V. A.; Pieper, U.; Stuart, A. C.; Marti-Renom, M. A.; Madhusudhan, M. S.; Yerkovich, B.; Sali, A. Tools for comparative protein structure modeling and analysis. *Nucleic Acids Res.* **2003**, *31*, 3375−3380.
(29) He, D.; Marles-Wright, J. Ferritin family proteins and their use in bionanotechnology. *New Biotechnol.* **2015**, *32*, 651−657.
(30) Oddo, A.; Mortensen, S.; Thøgersen, H.; De Maria, L.; Hennen, S.; McGuire, J. N.; Kofoed, J.; Linderoth, L.; Reedtz-Runge, S. alpha-Helix or beta-Turn? An Investigation into N-Terminally Constrained Analogues of Glucagon-like Peptide 1 (GLP-1) and Exendin-4. *Biochemistry* **2018**, *57*, 4148−4154.
(31) Ji, X. T.; Huang, L.; Lin, Q.; Huang, H. Q. Characteristics and Kinetics of Iron Releasefrom the Ferritin under the EGCG reduction. *Biol. Trace Elem. Res.* **2012**, *146*, 134−140.
(32) Wang, Y.; Chen, H.; Zang, J.; Zhang, X.; Zhao, G. Re-designing ferritin nanocages for mercuric ion detection. *Analyst* **2019**, *144*, 5890−5897.
(33) Fremaux, J.; Venin, C.; Mauran, L.; Zimmer, R. H.; Guichard, G.; Goudreau, S. R. Peptide-oligourea hybrids analogue of GLP-1 with improved action in vivo. *Nat. Commun.* **2019**, *10*, 924.
(34) Wang, Z.; Gao, H.; Zhang, Y.; Liu, G.; Niu, G.; Chen, X. Functional ferritin nanoparticles for biomedical applications. *Front. Chem. Sci. Eng.* **2017**, *11*, 633−646.
(35) Truffi, M.; Fiandra, L.; Sorrentino, L.; Monieri, M.; Corsi, F.; Mazzucchelli, S. Ferritin nanocages: A biological platform for drug delivery, imaging and theranostics in cancer. *Pharmacol. Res.* **2016**, *107*, 57−65.
(36) Bellapadrona, G.; Sinkar, S.; Sabanay, H.; Liljestrom, V.; Kostiainen, M.; Elbaum, M. Supramolecular Assembly and Coalescence of Ferritin Cages Driven by Designed Protein-Protein Interactions. *Biomacromolecules* **2015**, *16*, 2006−2011.
(37) Lee, B. R.; Ko, H. K.; Ryu, J. H.; Ahn, K. Y.; Lee, Y. H.; Oh, S. J.; Na, J. H.; Kim, T. W.; Byun, Y.; Kwon, I. C.; Kim, K.; Lee, J. Engineered Human Ferritin Nanoparticles for Direct Delivery of Tumor Antigens to Lymph Node and Cancer Immunotherapy. *Sci. Rep.* **2016**, *6*, 35182.
(38) Kanekiyo, M.; Wei, C. J.; Yassine, H. M.; McTamney, P. M.; Boyington, J. C.; Whittle, J. R.; Rao, S. S.; Kong, W. P.; Wang, L.; Nabel, G. J. Self-assembling influenza nanoparticle vaccines elicit broadly neutralizing H1N1 antibodies. *Nature* **2013**, *499*, 102−106.
(39) Falvo, E.; Tremante, E.; Fraioli, R.; Leonetti, C.; Zamparelli, C.; Boffi, A.; Morea, V.; Ceci, P.; Giacomini, P. Antibody-drug conjugates: targeting melanoma with cisplatin encapsulated in protein-cage nanoparticles based on human ferritin. *Nanoscale* **2013**, *5*, 12278−12285.
(40) Khoshnejad, M.; Shuvaev, V. V.; Pulsipher, K. W.; Dai, C.; Hood, E. D.; Arguiri, E.; Christofidou-Solomidou, M.; Dmochowski, I. J.; Greineder, C. F.; Muzykantov, V. R. Vascular Accessibility of Endothelial Targeted Ferritin Nanoparticles. *Bioconjugate Chem.* **2016**, *27*, 628−637.

https://dx.doi.org/10.1021/acs.molpharmaceut.0c00098
Mol. Pharmaceutics 2020, 17, 1663−1673

(41) Sanchez-Garcia, L.; Martin, L.; Mangues, R.; Ferrer-Miralles, N.; Vazquez, E.; Villaverde, A. Recombinant pharmaceuticals from microbial cells: a 2015 update. *Microb. Cell Fact.* **2016**, *15*, 33.
(42) Fan, K.; Gao, L.; Yan, X. Human ferritin for tumor detection and therapy. *Wiley Interdiscip. Rev. Nanomed. Nanobiotechnol.* **2013**, *5*, 287−298.
(43) Sharma, D.; Verma, S.; Vaidya, S.; Kalia, K.; Tiwari, V. Recent updates on GLP-1 agonists: Current advancements & challenges. *Biomed. Pharmacother.* **2018**, *108*, 952−962.
(44) Pi-Sunyer, X.; Astrup, A.; Fujioka, K.; Greenway, F.; Halpern, A.; Krempf, M.; Lau, D. C.W.; le Roux, C. W.; Violante Ortiz, R.; Jensen, C. B.ør.; Wilding, J. P.H. A Randomized, Controlled Trial of 3.0 mg of Liraglutide in Weight Management. *N. Engl. J. Med.* **2015**, *373*, 11−22.
(45) Davies, M. J.; Bergenstal, R.; Bode, B.; Kushner, R. F.; Lewin, A.; Skjøth, T. V.; Andreasen, A. H.; Jensen, C. B.ør.; DeFronzo, R. A. Efficacy of Liraglutide for Weight Loss Among Patients With Type 2 Diabetes: The SCALE Diabetes Randomized Clinical Trial. *JAMA* **2015**, *314*, 687−699.
(46) O'Neil, P. M.; Birkenfeld, A. L.; McGowan, B.; Mosenzon, O.; Pedersen, S. D.; Wharton, S.; Carson, C. G.; Jepsen, C. H.; Kabisch, M.; Wilding, J. P. H. Efficacy and safety of semaglutide compared with liraglutide and placebo for weight loss in patients with obesity: a randomised, double-blind, placebo and active controlled, dose-ranging, phase 2 trial. *Lancet* **2018**, *392*, 637−649.
(47) Soo Choi, H.; Liu, W.; Misra, P.; Tanaka, E.; Zimmer, J. P; Itty Ipe, B.; Bawendi, M. G; Frangioni, J. V Renal clearance of quantum dots. *Nat. Biotechnol.* **2007**, *25*, 1165−1170.
(48) Longmire, M.; Choyke, P. L.; Kobayashi, H. Clearance properties of nano-sized particles and molecules as imaging agents: considerations and caveats. *Nanomedicine (London, U. K.)* **2008**, *3*, 703−717.
(49) Tsukamoto, R.; Godonoga, M.; Matsuyama, R.; Igarashi, M.; Heddle, J. G.; Samukawa, S.; Yamashita, I. Effect of PEGylation on controllably spaced adsorption of ferritin molecules. *Langmuir* **2013**, *29*, 12737−12743.

https://dx.doi.org/10.1021/acs.molpharmaceut.0c00098
Mol. Pharmaceutics 2020, 17, 1663−1673